

Molecular Dynamics Study of a Hyperthermophilic and a Mesophilic Rubredoxin

Alessandro Grottesi,^{1,2*} Marc-Antoine Ceruso,² Alfredo Colosimo,¹ and Alfredo Di Nola²

¹Department of Biochemical Sciences, University of Rome, La Sapienza, Rome, Italy

²Department of Chemistry, University of Rome, La Sapienza, Rome, Italy

ABSTRACT In recent years, increased interest in the origin of protein thermal stability has gained attention both for its possible role in understanding the forces governing the folding of a protein and for the design of new highly stable engineered biocatalysts. To study the origin of thermostability, we have performed molecular dynamics simulations of two rubredoxins, from the mesophile *Clostridium pasteurianum* and from the hyperthermophile *Pyrococcus furiosus*. The simulations were carried out at two temperatures, 300 and 373 K, for each molecule. The length of the simulations was within the range of 6–7.2 ns. The rubredoxin from the hyperthermophilic organism was more flexible than its mesophilic counterpart at both temperatures; however, the overall flexibility of both molecules at their optimal growth temperature was the same, despite 59% sequence homology. The conformational space sampled by both molecules was larger at 300 K than at 373 K. The essential dynamics analysis showed that the principal overall motions of the two molecules are significantly different. On the contrary, each molecule showed similar directions of motion at both temperatures. *Proteins* 2002;46:287–294.

© 2002 Wiley-Liss, Inc.

Key words: essential dynamics; protein stability; thermostability; cooperativity; flexibility

INTRODUCTION

Enzymes that evolved from thermophile or hyperthermophile organisms have attracted considerable attention because they serve as paradigms for delineating the factors responsible for protein stability. Hyperthermophilic enzymes exhibit considerable potential for a number of biotechnological applications that require the use of high temperatures.^{1,2} However, no unifying theory to explain protein thermostability has been accepted because stability may arise with the interplay of many factors. In the case of aldehyde ferredoxin oxidoreductase, thermostability is associated with an increase in the packing density of the hydrophobic core and a decrease in internal cavities.³ The electrostatic contribution to the thermal stability of proteins in terms of salt bridges and networks of ion pairs has been demonstrated in the case of ferredoxins⁴ and more recently in the DNA-binding protein Sac7d from

Sulfolobus acidocaldarius.⁵ Other, commonly accepted, factors that switch a mesophilic protein to a thermophilic one, are: improved hydrogen bonding networks,⁶ stabilization of α -helices by α -helix capping,^{7,8} and shortening of loops between secondary structural elements.^{9,10} A set of cavity-creating single point mutations has been shown to increase the thermal stability of T4 lysozyme.¹¹ The role of a single amino acid mutation in the ribonuclease P2 from *Sulfolobus solfataricus* was found to be crucial for the conformational stability of the structure at high temperature and pressure.¹²

Nevertheless, it is often assumed that one of the most common strategies to enhance protein thermal resistance is to increase the rigidity of the molecular structure,^{13,14} although no direct relationship between protein thermal stability and protein flexibility can be stated a priori. Several studies have shown that proteins that belong to both thermophilic or hyperthermophilic organisms exhibit reduced structural flexibility at room temperature with respect to their mesophilic counterparts.^{15–18} In contrast, experimental observations of α -amylase¹⁹ and of esterase from the eubacterium *Bacillus acidocaldarius*,²⁰ as well as molecular dynamics (MD) simulations in subtilisin-E,²¹ show that proteins from thermophilic organisms are more flexible than their mesophilic homologues.

Computational approaches have been extensively used on both mesophilic and thermophilic proteins to study the temperature dependence of several quantities, such as the intraprotein Coulombic interaction,^{5,22} effect of point mutations,^{11,12} redox potential,²³ and flexibility.¹⁸ The length of MD simulations was within a few hundred picoseconds; in one case, it reached the nanosecond timescale.²¹

This article investigates the role played by internal dynamic fluctuations of the polypeptide chain for the stability of the native fold at room and high temperature. To answer this question, we have compared the dynamic

Grant sponsor: European Community Training and Mobility of Researchers Program (Protein Folding); Grant sponsor: MURST 99 (Structural Biology of Redox Proteins).

Marc-Antoine Ceruso is currently at the Department of Physiology and Biophysics, Mt. Sinai School of Medicine, New York, NY.

*Correspondence to: Alessandro Grottesi, c/o Alfredo Di Nola, Department of Chemistry, University of Rome La Sapienza, P.O. Box 34 Roma, 62 P.le Aldo Moro 5, Rome I-00185, Italy.
E-mail: grottesi@caspur.it

Received 15 June 2001; Accepted 9 October 2001

properties of two iron–sulfur rubredoxins (Rb) from *Pyrococcus furiosus* (RbPf), a hyperthermophilic archaeon that grows at ~ 100 °C, and *Clostridium pasteurianum* (RbCp), which grows at ~ 37 °C.

The flexibility of rubredoxins was investigated by Jung and coworkers,²⁴ with a 30-ps MD simulation. The investigators found that the hyperthermophilic rubredoxin is less flexible than the mesophilic form. A comparable result was achieved by Bradley et al.,²⁵ with a 10-ps MD simulation. Lazaridis et al.²⁶ performed a 400-ps MD simulation, followed by a 300-ps simulation, to study the unfolding behavior of both RbPf and rubredoxin from mesophile *Desulfovibrio vulgaris* up to 500 K.

The presence of four additional residues that adopt a β -sheet conformation has been considered the main origin of thermostability in rubredoxins.²⁷ The x-ray-based study also showed that the presence of a Glu instead of a Pro in the primary structure of RbPf gives rise to a salt bridge that also involves residues Ala-1 and Phe-29. It was found that the side-chain of Lys-6 is linked to Glu-49 by means of a salt bridge, and that this linkage apparently contributes to the difference in thermal stability between the two homologous rubredoxins.²⁸ However, the results obtained from the comparison between RbPf and the remaining elements of a whole set of rubredoxins from mesophilic bacteria²⁹ appear to exclude the role of specific amino acids to explain the extraordinary thermal stability of RbPf. In agreement with an earlier study by Eidsness et al.,³⁰ Giuliani et al.²⁹ conclude that global interactions (i.e., spread over the whole molecule), more than local stabilizing interactions, should be considered in the case at hand.

The present study reports the results of four MD simulations (6–7.2 ns long) on RbCp and RbPf at two characteristic temperatures of growth; 300 and 373 K, respectively. The principal finding is that although both proteins share about 59% sequence identity, the hyperthermophilic rubredoxin is more flexible than the mesophilic rubredoxin at both simulated temperatures. However, both proteins have the same overall flexibility at their optimal growth temperature. The conformational space sampled by both molecules is larger at 300 K than at 373 K. Finally, essential dynamics analysis of the trajectories shows that the internal motions of the two proteins are significantly different.

MATERIALS AND METHODS

Definitions

RbPf300 and RbPf373 designate the MD simulations of rubredoxin from hyperthermophile *Pyrococcus furiosus* at 300 and 373 K, respectively, whereas RbCp300 and RbCp373 stand for the corresponding MD simulations of rubredoxin from mesophile *Clostridium pasteurianum* at 300 and 373 K, respectively. In Figures 1–7 and Tables I and II, the numbering of the primary structures is the one corresponding to RbCp. According to the sequence alignment between the two molecules, the numbering of primary structure in RbPf is shifted downward by one unit.

Molecular Dynamics

The starting configurations for both hyperthermophilic and mesophilic rubredoxins were obtained from the Protein Data Bank (PDB), entry code 1IRO⁴⁴ and 1CAA²⁷ for *Clostridium pasteurianum* and *Pyrococcus furiosus* rubredoxins, respectively. The reference bond angles and distances around the iron atom of the FeS₄ cluster were taken from the crystal structures of the proteins in their oxidized state. The simulations were performed in the NVT ensemble, using the GROMACS simulation software packages,³¹ implemented on a parallel architecture. A modification of the GROMOS87 force field was used with additional terms for aromatic hydrogens³² and improved carbon–oxygen interaction parameters.³³ The SHAKE algorithm³⁴ was used to constrain bond lengths, with a time step of 2 fs. All starting structures were immersed in a rectangular box of SPC water molecules.³⁵ All simulations were performed with a periodic boundary condition at the desired temperature using an external bath³⁶ with a coupling constant $\tau = 0.002$ ps, equal to the integration timestep. Nonbonded cutoffs of 1.0 nm and 1.4 nm for Lennard-Jones and Coulomb potentials, respectively, were used. The pair lists were updated every 10 steps. For all systems, the solvent was relaxed by energy minimization, followed by 10 ps of MD at 300 K, while restraining protein atomic positions with a harmonic potential. The systems were then minimized without restraints and their temperature brought to 300 K in a stepwise manner: 10-ps-long MD runs were carried out at 50, 100, 200, and 250 K before the production runs were started at 300 K. An initial configuration set for simulations at 373 K was taken from the configuration after 2,000 ps of simulations at 300 K for both systems. This structure was gradually brought to 373 K in a similar manner with respect to the first thermalization. The total length of the simulations was 7.2 ns at 300 K and 6.0 ns at 373 K. For both systems at both temperatures, the structures of the trajectories were collected every 0.1 ps. Secondary structure content was calculated using the software Dictionary of Secondary Structure of Protein (DSSP).³⁷ The root-mean-square deviation (RMSD) of a selected element with respect to its reference value is defined as

$$\text{RMSD} = \sqrt{\frac{1}{N} \sum_{i=1}^N (\mathbf{r}_i - \mathbf{r}_0)^2}$$

where \mathbf{r}_i represents the element position at time i and \mathbf{r}_0 the reference value. The root-mean-square fluctuation (RMSF) of a selected element with respect to its average value is defined as

$$\text{RMSF} = \sqrt{\frac{1}{N} \sum_{i=1}^N (\mathbf{r}_i - \langle \mathbf{r} \rangle)^2}$$

where \mathbf{r}_i represents the element position at time i and $\langle \mathbf{r} \rangle$ the average value.

Essential Dynamics

Quantitative characterization of the dynamic properties of each system relied on principal component analysis of the covariance matrix of the positional fluctuations of the C_{α} atoms.^{38–40} The covariance matrix was built from the equilibrated portion of the trajectories, and its diagonalization afforded the principal directions of the large-amplitude concerted motions (principal eigenvectors) that characterize the essential subspace of the internal dynamics of a protein. The dynamic signature of a protein was defined by the subspace corresponding to the first 10 eigenvectors with largest eigenvalues of the covariance matrix of the fluctuations.

Comparison of the dynamic properties of two proteins was obtained by the root-mean-square inner product, RMSIP, between the corresponding dynamic signatures (first 10 eigenvectors).^{41,42}

$$\text{RMSIP} = \sqrt{\frac{1}{10} \sum_{i=1}^{10} \sum_{j=1}^{10} (\eta_i^a \cdot \eta_j^b)^2}$$

where η_i^a and η_j^b are the i th and j th eigenvectors from set a (first protein) and set b (second protein), respectively.

RESULTS AND DISCUSSION

Comparison of Starting Structures

The structure of RbPp has been determined both in solution, by nuclear magnetic resonance (NMR) spectroscopy,⁴³ and in the crystal, by x-ray crystallography.²⁷ The three-dimensional structure of RbCp has been elucidated by x-ray crystallography.⁴⁴ Both molecules (Fig. 1) consist of 53 residues, belonging to the mainly β class^{45,46} and containing four cysteine residues bound to an iron atom to form a loop structure, commonly defined as a “knuckle” (Cys-X-X-Cys-X-X).⁴⁷ Their primary structures are 59% identical with RMS displacement of their C_{α} positions of 0.05 nm in best aligned regions. Rubredoxin from RbPp has a higher β -sheet content than its mesophilic counterpart: residues 1–6, 9–14, and 47–51, for RbPp,²⁷ and residues 4–6, 11–14, and 49–51 for RbCp,⁴⁴ respectively.

Global Structural Stability

The potential interaction energies (solute/solute + solute/solvent) trajectories are shown in Figure 2. The energies are approximately constant at 300 K over the whole simulation. At 373 K, a constant value is reached within the first 300 ps of the simulation. As reported in the experimental section, the initial coordinates for the simulations at 373 K were taken from the conformation after 2 ns of simulation at 300 K.

Figure 3 shows the trajectories of the RMSD with respect to the crystal structure. At 300 K, the RMSD increases up to an equilibrium value of 0.27 and 0.19 nm for RbPp and RbCp, respectively. At 373 K, the RMSD has an almost constant value of 0.28 and 0.21 nm for RbPp and RbCp, respectively. The largest deviations at both temperatures for RbPp are localized on residues

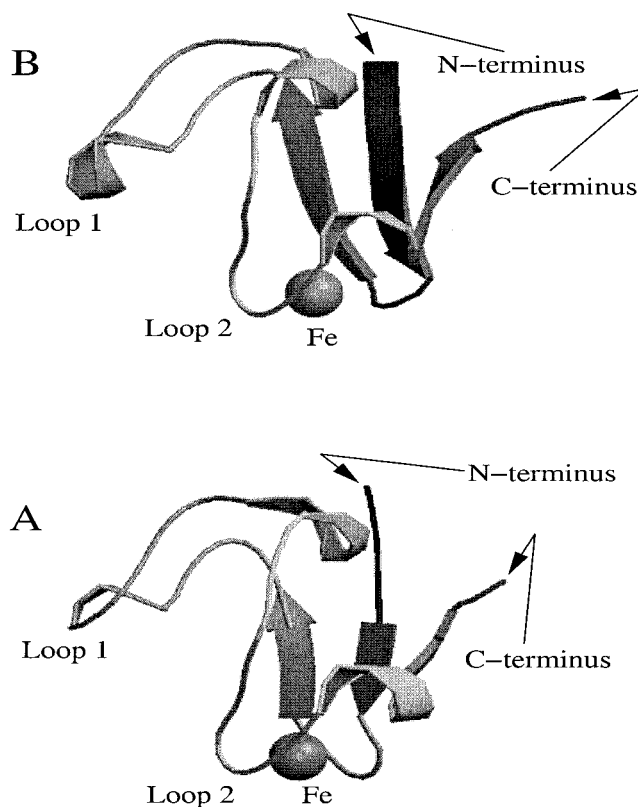


Fig. 1. Graphic representation of the molecular structure of rubredoxin from *Clostridium pasteurianum* (A) and *Pyrococcus furiosus* (B) in their oxidized state. Picture generated using Molscript⁵⁰ and Raster3D software.⁵¹

22–28 and 30–37; for RbCp, they are localized in residues 21–24 and 41–45. It should be pointed out that, at equilibrium, the protein samples different regions in the allowed conformational space, so that the RMSD can show a damped profile. The subsequent analyses have been performed by discarding the first 1.2 ns for the simulations at 300 K and the first 0.5 ns for the simulations at 373 K.

Despite these deviations that occur in the molecular structure, both rubredoxins do not undergo significant unfolding processes, as evidenced by the radius of gyration (data not shown) and by the secondary structure content calculated during the simulations (Table I). Table I reports the average number of residues in a given secondary structure calculated by DSSP.³⁷ For comparison, the DSSP values for the PDB structure and for the energy-minimized structure are reported. Both systems retain most of their crystallographic secondary structures at 300 K, with only the 3_{10} -helix content reduced during the simulations. Interestingly, at 373 K, RbCp loses a residue in the β -sheet conformation, whereas RbPp gains one residue in the same secondary structure.

Dynamics

Figure 4 compares the RMSF of RbPp and RbCp on a residue basis, at both temperatures. The first interesting

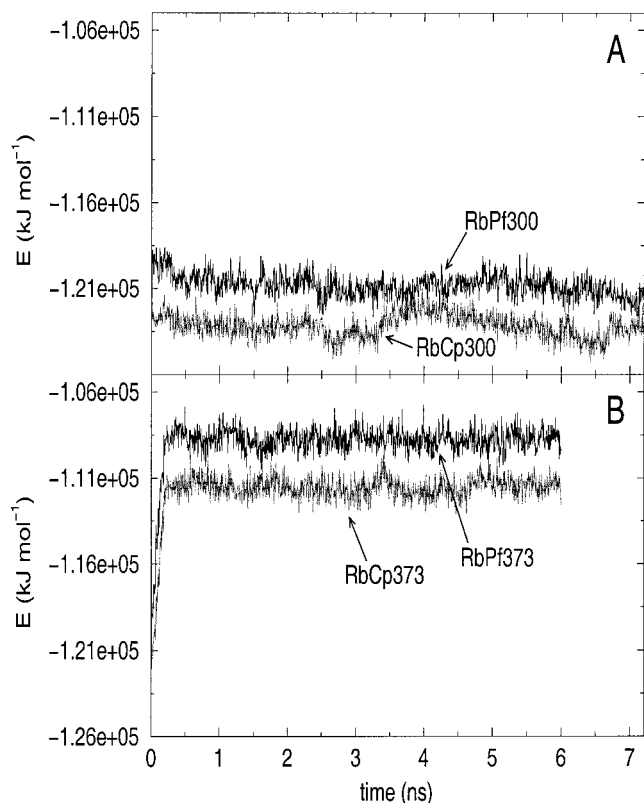


Fig. 2. Trajectories of the potential interaction energy (solute/solute + solute/solvent) of RbPf and RbCp at 300 K (A) and 373 K (B) over the whole trajectories.

result is that RbPf is more flexible than its mesophilic counterpart at both temperatures. This result is in agreement with that observed experimentally in esterase,²⁰ from *Bacillus acidocaldarius*, and α -amylase,¹⁹ in which thermostability is experimentally related to higher flexibility, and by MD simulation in subtilisin-E.²¹

The overall flexibility can be calculated by the trace of the diagonalized covariance matrix of the atomic positional fluctuations. We have obtained the following values for RbCp: 0.60 nm² at 300 K and 0.42 nm² at 373 K. Similarly for RbPf we had 1.12 nm² at 300 K and 0.67 nm² at 373 K, thus confirming what shown in Figure 4. It should be pointed out that the overall flexibility of both molecules at their growth temperature is almost the same: 0.60 nm² for RbCp300 and 0.67 nm² for RbPf373. It is worth noting that the calculated flexibility of both RbCp373 and RbPf373 is smaller than the corresponding flexibility at 300 K.

This apparent paradox can be explained in terms of conformational space sampling, as can be observed by the essential dynamics analysis. Figure 5 shows that, at 300 K, at least two subspaces are sampled, while at 373 K only one subspace is sampled. The projection of the trajectories at 373 K onto the eigenvectors obtained at 300 K provides evidence that the subspace at 373 K for RbCp [Fig. 5(C)] is close to region 2 of Figure 5(A) and the subspace at 373 K

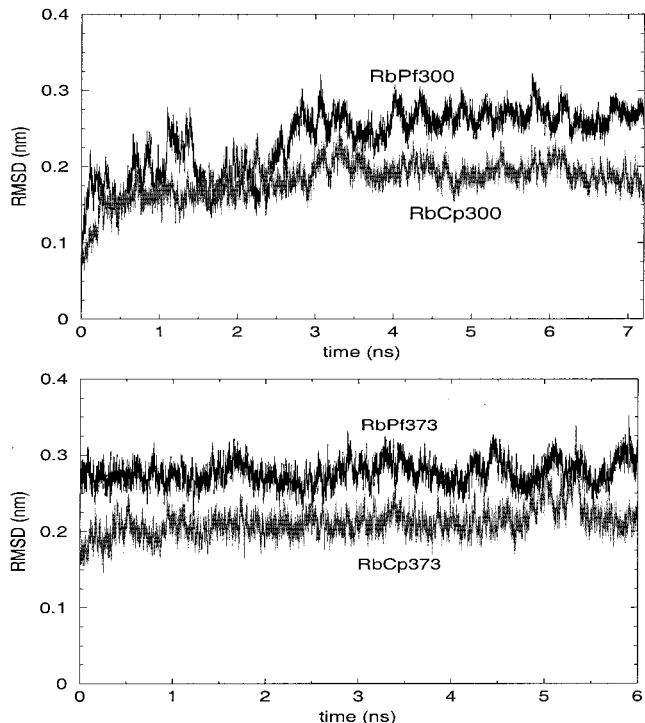


Fig. 3. Trajectory of the root-mean-square deviation with respect to the crystal structure of hyperthermophilic RbPf (black) and mesophilic RbCp (gray) rubredoxin at 300 K (top) and 373 K (bottom). The thermalization time from 300 up to 373 K is not shown.

for RbPf [Fig. 5(D)] is close to region 2 of Figure 5(B). It should be pointed out that the eigenvectors at 373 K [Fig. 5(E,F)], although close, do not coincide with those at 300 K. Thus, it can be concluded that, at high temperature, only one subspace, among those allowed at room temperature, is sampled. This can be explained in terms of conformational entropy: at 300 K, we have almost equivalent free energy minima, with different entropy values. At high temperature, the low entropy minima are less populated on respect to the high entropy minima. Within each minimum the fluctuation is larger at 373 K than at 300 K, as expected.

To characterize the structural differences among the two regions at 300 K, we have compared the RMSD of their C α atoms with respect to the crystal structure. The results are reported in Figure 6. For RbCp (Fig. 6, bottom), the two structures differ in region 36–43, that includes the two catalytic cysteines, 39 and 42, of the active site. Briefly, the protein region responsible for the large sampled space at 300 K involves primarily loops 1 and 2 of the mesophilic rubredoxin.

The comparison between the two regions of RbPf (Fig. 6, top) at 300 K shows that they differ in the stretch 19–38. This deviation is caused by a rigid-body displacement of the loop 1 with respect to the stretch of residues ranging from 29 to 38. The amino acids with large RMSD in both molecules largely correspond to the region with recurrent hydrophobic residue content, as detected by Giuliani et

TABLE I. Average Number of Residues in a Given Secondary Structure of RbPf and RbCp Calculated in the Equilibrated Part of the Trajectories at 300 K and 373 K, According to DSSP Software*

	RbPf				RbCp			
	300 K	373 K	X-ray	min	300 K	373 K	X-ray	min
3_{10} -helix	3.0 (0.7)	2.7 (1.1)	9	3	3.3 (1.3)	0.3 (1.0)	9	6
β -Sheet	9.7 (1.4)	10.7 (1.6)	10	10	9.2 (1.2)	8.7 (0.7)	8	8
Bridge	0.7 (1.4)	1.6 (1.3)	4	4	0.6 (0.9)	0.0 (0.0)	4	4
Bend	13.1 (3.1)	8.3 (3.1)	2	2	13.3 (2.2)	14.1 (1.8)	1	1
Turn	6.5 (3.5)	10.1 (2.8)	14	20	9.1 (2.6)	11.8 (1.4)	14	17
Coil	20.1 (3.2)	19.5 (2.5)	14	14	17.6 (2.5)	18.0 (1.4)	17	17

RbPf, rubredoxin *Pyrococcus furiosus*; RbCp, rubredoxin *Clostridium pasteurianum*.

*Standard deviations are given in parentheses. The corresponding reference values in the crystal structure and the values in the energy-minimized starting structure are also reported.

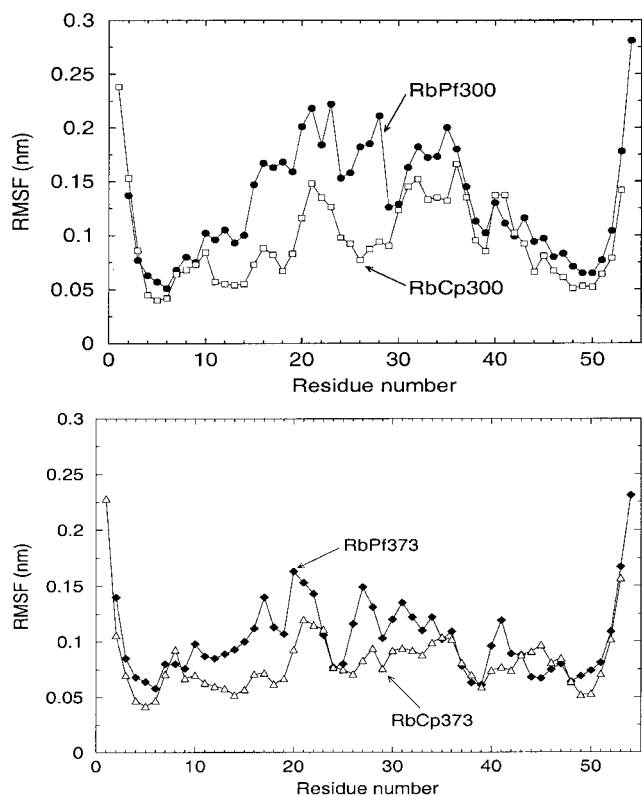


Fig. 4. Root-mean-square fluctuations per residue of RbPf and RbCp computed at 300 K (top) and 373 K (bottom). ●, RbPf300; ◆, RbPf373; □, RbCp300; △, RbCp373.

al.²⁹ by a recurrence quantification analysis (RQA). According to Giuliani et al.,²⁹ the recurrent hydrophobicity patterns involves in RbCp residues 5–10 and 37–42; in RbPf residues 6–10, 22–25, 27–29, 35–38, 40–42, and 46–48.

The overall concerted motions of the two proteins at both temperatures were monitored by the essential dynamics analysis.⁴⁰ Table II reports the comparison of the essential subspaces of the proteins. We calculated the root-mean-square inner product RMSIP (see Materials and Methods) between the first 10 eigenvectors of each simulation. It has

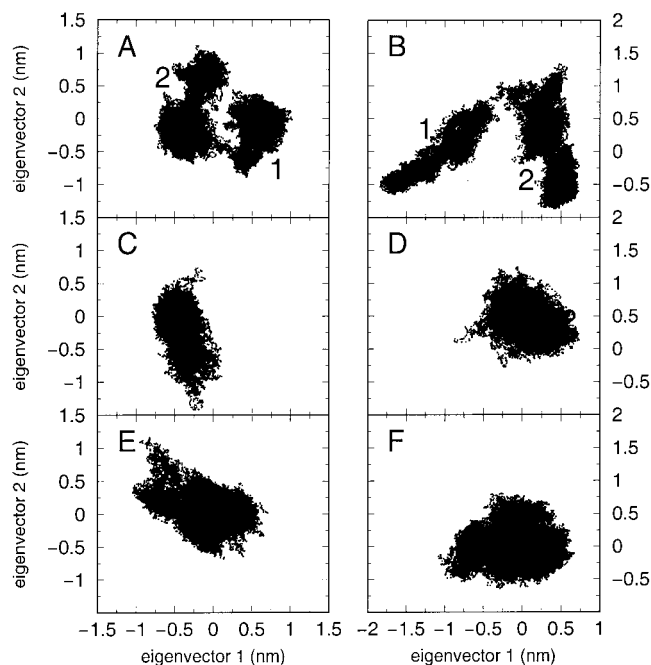


Fig. 5. Projection of the C_{α} atoms trajectory along the first two principal components of the covariance fluctuations matrix of the RbCp (A) and RbPf (B) at 300 K. The numbers indicate different regions. C,D: Projections of the trajectories at 373 K onto the principal components of A and B, respectively. E,F: Projection of the trajectories of RbCp (E) and RbPf (F) at 373 K onto their first two eigenvectors.

been reported^{48,49} that this number accounts for the (dis)similarity of the essential motions. For reference values, we have divided each trajectory in two halves and have calculated the inner product between the first 10 essential eigenvectors of each half. The values obtained represent the expected reference values that indicate a similarity in the motions and are taken as thresholds for a comparison among different trajectories. We have therefore calculated the inner product between the equilibrated part of the trajectories of the two molecules at the two temperatures. The results show that each molecule has similar motions at both temperatures. On the contrary, the motions of the different rubredoxins are

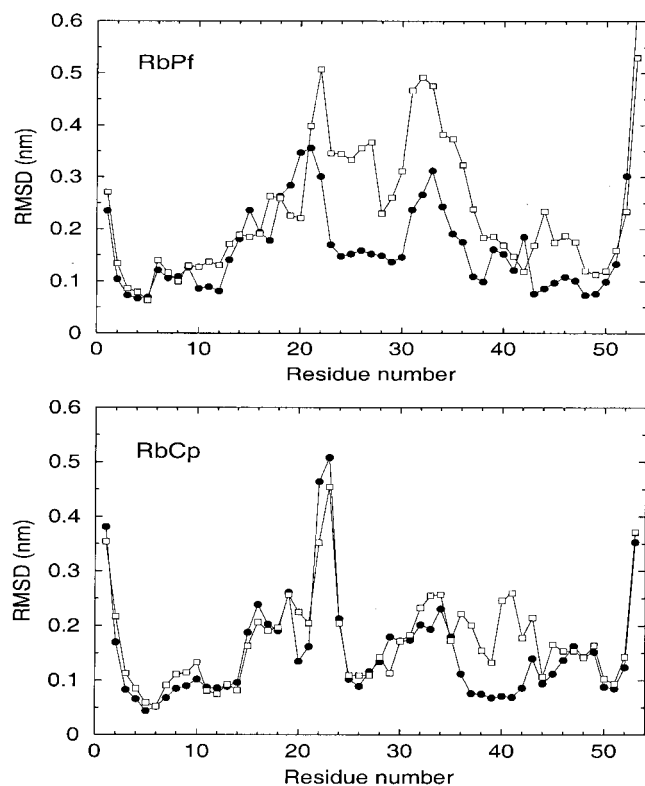


Fig. 6. Root-mean-square deviation per residue with respect to the crystal structure of RbCp (bottom) and RbPf (top) calculated within each region of Figure 5A and B. RbCp300: region 1 (●); region 2 (□). RbPf300: region 1 (●), region 2 (□).

TABLE II. Root-Mean-Square Inner Product Between the First 10 Eigenvectors of Different Trajectories

	RbCp300	RbCp373	RbPf300	RbPf373
RbCp300	0.765 ^a	0.774	0.465	0.412
RbCp373	—	0.865 ^a	0.474	0.470
RbPf300	—	—	0.712 ^a	0.740
RbPf373	—	—	—	0.778 ^a

RbCp, rubredoxin *Clostridium pasteurianum*; RbPf, rubredoxin *Pyrococcus furiosus*.

^aThese values refer to the RMSIP obtained by comparing the two halves of the corresponding trajectory.

significantly different when compared at both simulated temperatures.

Figure 7 illustrates the motion along the first eigenvector at 300 K. It should be noted that the motion of loops 1 and 2 is different in the two molecules. In fact, in RbCp it leads to partial exposure of the core of the protein to the solvent, which also affects the active site, by orthogonally sliding loop 2 with respect to the β -sheet plane, a movement previously observed in Jung et al.²⁴ On the contrary, in RbPf the principal motion at 300 K is due to the translation of loop 1 toward the core of the protein, which is coupled to a concerted motion of the 29–38 stretch in the opposite direction. It is important to note that the active site region is not altered by these motions.

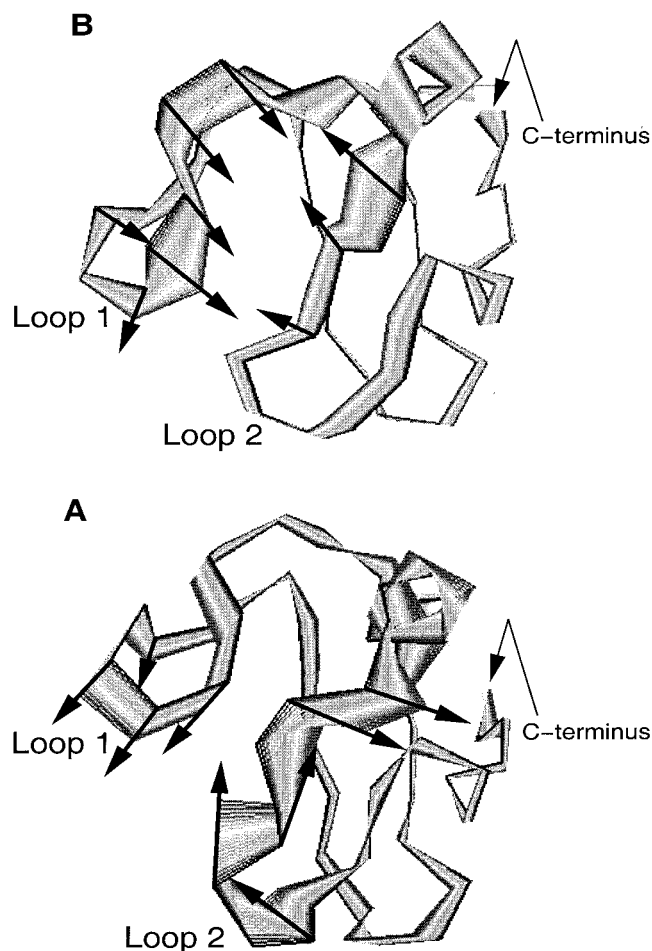


Fig. 7. Projection of the motions along the first eigenvector at 300 K. A: RbCp. B: RbPf. Arrows, direction of the motion.

CONCLUSIONS

We report the results obtained by long MD simulations of two rubredoxins from mesophilic (RbCp) and hyperthermophilic (RbPf) organisms. The aim was to study the structural and dynamic differences between the two enzymes.

Within the time scale of the simulations, we show that the flexibility of the protein from the hyperthermophilic organism is larger than its mesophilic counterpart. This finding is in agreement with reported experimental data on α -amylase¹⁹ and esterase²⁰ and MD data on subtilisin-E.²¹ This represents a novelty with respect to the most common theory of thermostability. Previous MD simulations on rubredoxins of few tens of picoseconds^{24,25} yielded opposing conclusions, most certainly due to the different length of the simulations, which in the present case is a few nanoseconds.

The overall flexibility of both molecules at their optimal temperature of growth is the same, as evidenced by the trace of the diagonalized covariance matrix of atomic fluctuations. This coincidence could be related to the optimal activity of each molecule.

Another (quite surprising) result was obtained analyzing the conformational space sampled by the two proteins at different temperatures: two regions were sampled at low temperature and only one at high temperature (see Fig. 5). This behavior can be attributable to different conformational entropy of the allowed sampled minima at 300 K; thus, at higher temperature, the region with higher entropy values is more populated.

The essential dynamics analysis shows that the internal motions of each protein are similar at both temperatures. By contrast, the principal motions are significantly different in the two proteins.

We can conclude that, according to this picture, the thermostability in rubredoxin is obtained by a different dynamic behavior of the hyperthermophilic protein with respect to the mesophilic protein. The greater flexibility facilitates its adaptation to the larger kinetic energy. The difference in flexibility is coupled to a difference in the directions of internal motions.

REFERENCES

- Adams MWW, Perler FB, Kelly RM. Extremozymes: expanding the limits of biocatalysis. *Biotechnology* 1995;13:662–668.
- Adams MWW, Kelly RM. Finding and using hyperthermophilic enzymes. *Trends Biotechnol* 1998;16:329–332.
- Chan MK, Mukund S, Kletzin A, Adams MWW, Rees DC. Structure of a hyperthermophilic tungstopterin enzyme, aldehyde ferredoxin oxidoreductase. *Science* 1995;267:1463–1469.
- Perutz MF, Raidt H. Stereochemical basis of heat stability in bacterial ferredoxins and in hemoglobin A2. *Nature* 1975;255:256–259.
- de Bakker PIW, Hünenberger PH, McCammon JA. Molecular dynamics simulations of the hyperthermophilic protein Sac7d from *Sulfolobus acidocaldarius*: contribution of salt bridges to thermostability. *J Mol Biol* 1999;285:1811–1830.
- Shih P, Kirsch JF. Design and structural analysis of an engineered thermostable chicken lysozyme. *Protein Sci* 1995;4:2063–2072.
- Facchiano AM, Colonna G, Ragone R. Helix stabilizing factors and stabilization of thermophilic proteins: an X-ray based study. *Protein Eng* 1998;11:753–760.
- Petukhov M, Kil Y, Kuramitsu S, Lanzov V. Insights into thermal resistance of proteins from the intrinsic stability of their α -helices. *Proteins* 1997;29:309–320.
- Hardy F, Vriend G, van Der Vinne B, Frigerio F, Grandi G, Venema G, Eijsink VGH. The effect of engineering surface loops on the thermal stability of *Bacillus subtilis* neutral protease. *Protein Eng* 1994;7:425–430.
- Thompson MJ, Eisenberg D. Transproteomic evidence of a loop-deletion mechanism for enhancing protein thermostability. *J Mol Biol* 1999;290:595–604.
- Matthews BW. Studies on protein stability with T4 lysozyme. *Adv Protein Chem* 1995;46:249–278.
- Mombelli E, Afshar M, Fusi P, Mariani M, Tortora P, Connelly JP, Lange R. The role of phenylalanine 31 in maintaining the conformational stability of ribonuclease P2 from *Sulfolobus solfataricus* under extreme conditions of temperature and pressure. *Biochemistry* 1997;36:8733–8742.
- Giver L, Gershenson A, Freskgard PO, Arnold FH. Directed evolution of a thermostable esterase. *Proc Natl Acad Sci USA* 1998;95:12809–12813.
- Van den Burg B, Vriend G, Veltman OR, Venema G, Eijsink VGH. Engineering an enzyme to resist boiling. *Proc Natl Acad Sci USA* 1998;95:2056–2060.
- Veronese FM, Boccu E, Schiavon O, Grandi C, Fontana A. General stability of thermophilic enzymes: studies on 6-phosphogluconate dehydrogenase from *Bacillus stearothermophilus* and yeast. *J Appl Biochem* 1984;6:39–47.
- Wrba A, Schweiger A, Schultes V, Jaenicke R, Zavodsky P. Extremely thermostable D-glyceraldehyde-3-phosphate dehydrogenase from the eubacterium *Thermotoga maritima*. *Biochemistry* 1990;29:7584–7592.
- Kanaya S, Itaya M. Expression, purification, and characterization of a recombinant ribonuclease H from *Thermus thermophilus* HB8. *J Biol Chem* 1992;267:10184–10192.
- Vieille C, Zeikus JG. Thermozymes: identifying molecular determinants of protein structural and functional stability. *Trends Biotechnol* 1996;14:183–190.
- Fitter J, Heberle J. Structural equilibrium fluctuations in mesophilic and thermophilic α -amylase. *Biophys J* 2000;79:1629–1636.
- D'Auria S, Herman P, Lakowicz JR, Tanfani F, Bertoli E, Manco G, Rossi M. The esterase from the thermophilic eubacterium *Bacillus acidocaldarius*: structural-functional relationship and comparison with the esterase from the hyperthermophilic archaeon *Archaeoglobus fulgidus*. *Proteins* 2000;40:473–481.
- Colombo G, Merz KM Jr. Stability and activity of mesophilic subtilisin E and its thermophilic homolog: insights from molecular dynamics simulations. *J Am Chem Soc* 1999;121:6895–6903.
- Vetriani C, Maeder DL, Tolliday N, Yip KSP, Stillman TJ, Britton KL, Rice DW, Klump HH, Robb FT. Protein thermostability above 100°C: a key role for ionic interactions. *Proc Natl Acad Sci USA* 1998;95:12300–12305.
- Swartz PD, Ichiye T. Temperature dependence of the redox potential of rubredoxin from *Pyrococcus furiosus*: a molecular dynamics study. *Biochemistry* 1996;35:13772–13779.
- Jung DH, Kang NS, Jhon MS. Site-directed mutation study on hyperthermostability of rubredoxin from *Pyrococcus furiosus* using molecular dynamics simulations in solution. *J Phys Chem A* 1997;101:466–471.
- Bradley EA, Stewart DE, Wampler JE, Adams MWW. Investigations of the thermostability of rubredoxin models using molecular dynamics simulations. *Protein Sci* 1993;2:650–665.
- Lazaridis T, Lee I, Karplus M. Dynamics and unfolding pathways of a hyperthermophilic and mesophilic rubredoxin. *Protein Sci* 1997;6:2589–2605.
- Day MW, Hsu BT, Joshua-Tor L, Park JB, Zhou ZH, Adams MWW, Rees DC. X-ray crystal structures of the oxidized and reduced forms of the rubredoxin from the marine hyperthermophile archaeobacterium *Pyrococcus furiosus*. *Protein Sci* 1992;1:1494–1507.
- Bau R, Rees DC, Kurtz DM Jr, Scott RA, Huang H, Adams MWW, Eidsness MK. Crystal structure of rubredoxin from *Pyrococcus furiosus* at 0.95 Å resolution, and the structure of N-terminal methionine and formylmethionine variants of PfRd. Contribution of N-terminal interactions to thermostability. *J Biol Inorg Chem* 1998;3:484–493.
- Giuliani A, Benigni R, Sirabella P, Zbilut JP, Colosimo A. Nonlinear methods in the analysis of protein sequences: a case study in rubredoxins. *Biophys J* 2000;78:136–149.
- Eidsness MKA, Richie AE, Burden DN, Kurtz DM, Scott DA. Dissecting the contribution to the thermostability of *Pyrococcus furiosus* rubredoxins: β -sheet chimeras. *Biochemistry* 1997;36:10406–10413.
- van der Spoel D, Berendsen HJC, van Buuren AR, Apol MEF, Meulenhoff PJ, Sijbers ALTM. Gromacs user manual. The Netherlands: Nijenborgh 4, 9747 AG Groningen; 1995.
- van Gunsteren WF, Billeter SR, Eising AA, Hünenberger PH, Küger P, Mark AE, Scott WRP, Tironi IG. The GROMOS96 manual and user guide. Zurich: Biomos B.V.; 1996.
- van Buuren AR, Marrink SJ, Berendsen HJC. A molecular dynamics study of the decane/water interface. *J Phys Chem* 1993;97:9206–9212.
- Ryckaert JP, Ciccotti G, Berendsen HJC. Numerical integration of the cartesian equations of motion of a system with constraints: molecular dynamics of *n*-alkanes. *J Comp Phys* 1977;23:327–341.
- Berendsen HJC, Postma JPM, van Gunsteren WF, Hermans J. Interaction models for water in relation to protein hydration. Dordrecht: Reidel; 1981. p 331–342.
- Berendsen HJC, Postma JPM, van Gunsteren WF, Di Nola A, Haak JR. Molecular dynamics with coupling to an external bath. *J Chem Phys* 1984;81:3684–3690.

37. Kabsch W, Sander C. Dictionary of protein secondary structure: pattern recognition of hydrogen-bonded and geometrical features. *Biopolymers* 1983;22:2577–2637.
38. Garcia AE. Large-amplitude nonlinear motions in proteins. *Phys Rev Lett* 1992;68:2696–2699.
39. Wong CF, Zheng C, Shen J, McCammon A, Wolynes PG. Cytochrome c: a molecular proving ground for computer simulations. *J Phys Chem* 1993;97:3100–3110.
40. Amadei A, Linssen ABM, Berendsen HJC. Essential dynamics of proteins. *Proteins* 1993;17:412–425.
41. de Groot BL, van Aalten DMF, Amadei A, Berendsen HJC. The consistency of large concerted motions in proteins in molecular dynamics simulations. *Biophys J* 1996;71:1707–1713.
42. van Aalten DMF, de Groot BL, Berendsen HJC, Findlay JBC, Amadei A. A comparison of techniques for calculating protein essential dynamics. *J Comp Chem* 1997;18:169–181.
43. Blake PR, Park JB, Zhou ZH, Hare DR, Adams MWW, Summers MF. Solution-state structure by NMR of zinc-substituted rubredoxin from the marine hyperthermophilic archaeobacterium *Pyrococcus furiosus*. *Protein Sci* 1992;1:1508–1521.
44. Dauter Z, Wilson KS, Sieker LC, Moulis JM, Meyer J. Zinc- and iron-rubredoxins from *Clostridium pasteurianum* at atomic resolution: a high-precision model of a ZnS_4 coordination unit in a protein. *Proc Natl Acad Sci USA* 1996;93:8836–8840.
45. Orengo CA, Michie AD, Jones S, Jones DT, Swindells MB, Thornton JM. CATH—a hierarchic classification of protein domain structures. *Structure* 1997;5:1093–1108.
46. Pearl FMG, Lee D, Bray JE, Sillitoe I, Todd AE, Harrison AP, Thornton JM, Orengo CA. Assigning genomic sequences to CATH. *Nucleic Acids Res* 2000;28:277–282.
47. Schwabe JWR, Klug A. Zinc mining for protein domains. *Nature Struct Biol* 1994;1:345–349.
48. Ceruso MA, Amadei A, Di Nola A. Mechanics and dynamics of B1 domain of protein G: role of packing and surface hydrophobic residues. *Protein Sci* 1999;8:147–160.
49. Ceruso MA, Grottesi A, Di Nola A. Effects of core-packing on the structure, function and mechanics of a four-helix-bundle protein ROP. *Proteins* 1999;36:436–446.
50. Kraulis PJ. Molscript: a program to produce both detailed and schematic plots of protein structures. *J Appl Crystallogr* 1991;24:946–950.
51. Merritt EA, Bacon DJ. Raster3D: photorealistic molecular graphics. *Methods Enzymol* 1997;277:505–524.